JOURNAL OF GEOPHYSICAL RESEARCH, VOL. 112, D14206, doi:10.1029/2007JD008535, 2007

Information content of near-infrared spaceborne multiangular polarization measurements for aerosol retrievals

Matthew D. Lebsock,[1] Tristan S. L'Ecuyer,[1] and Graeme L. Stephens[1]

Received 10 February 2007; revised 1 May 2007; accepted 21 May 2007; published 25 July 2007.

[1] The information content of near-infrared spectral multiangular polarization measurements, utilized in the POLDER operational aerosol algorithm, for retrieving aerosol microphysical and optical properties is assessed. It is found that spectral measurements contain just one unique piece of microphysical information, while multiangular measurements add a second and polarization observations permit the constraint of a third microphysical parameter. In addition, it is demonstrated that the relationship between the aerosol single scattering properties and the aerosol microphysical parameters is nonunique. The implications of these findings for aerosol microphysical retrievals are demonstrated through the development of a retrieval for the aerosol optical depth, the index of refraction and a parameter describing the ratio of the number concentration of accumulation mode aerosols to those in the coarse mode. Application of the technique centers on the explicit weighting of individual measurements by rigorous estimates of their uncertainties offering the benefit of a realistic, dynamic retrieval error estimate. The aerosol optical depth, refractive index and number concentration ratio can respectively be estimated to within 15%, 5% and one order of magnitude over oceans. Error estimates are shown to increase by 50% over a mixed forest land surface type. The results further highlight a possible limitation of the measurements at low optical depths below 0.1 where the retrieval errors approach 100% for the optical depth and index of refraction and several orders of magnitude for the number concentration ratio.

Citation: Lebsock, M. D., T. S. L'Ecuyer, and G. L. Stephens (2007), Information content of near-infrared spaceborne multiangular polarization measurements for aerosol retrievals, *J. Geophys. Res.*, *112*, D14206, doi:10.1029/2007JD008535.

1. Introduction

[2] Understanding and quantifying the effects of aerosols on the climate system remains a significant challenge for the scientific community. Three primary pathways for the interaction of aerosols with the climate system have been identified in the literature [*King et al.*, 1999]. The first order, direct effect, of aerosols is to scatter and absorb incident solar radiation thus impacting heating rates and subsequently altering the atmospheric circulation. It has also been proposed that aerosols have a secondary, or indirect effect, on atmospheric radiation through their interaction with cloud droplet size distributions and precipitation [*Twomey*, 1977; *Albrecht*, 1989]. A third pathway is through indirect effects on heterogeneous atmospheric chemistry that can alter the chemical composition of radiatively active gases. Despite the importance of these impacts, the radiative effects due to anthropogenic modification of aerosol concentrations are among the least certain of any single climate forcing [*Intergovernmental Panel on Climate Change*, 2001]. The large uncertainty stems from several sources [*Schwartz*, 2004]. First, there are difficulties in quantifying the increase in aerosol number concentrations due to anthropogenic effects relative to natural sources. In addition, a reliable global aerosol climatology has yet to be developed. Finally, the secondary effects of aerosols on the climate have proven to be difficult to observe and quantify with any reliability.

[3] Satellite observations offer a potential to mitigate many of these issues through the global monitoring of aerosol properties and their interactions with the climate system. It is, however, first necessary to asses the accuracy and limitations of all satellite based retrievals to facilitate quantitative comparisons of different aerosol products and also to establish the statistical significance of any findings that make use of these products. Characterizing uncertainty in remotely derived aerosol products in turn necessitates an understanding of the physics that connects the directly observed quantities to the retrieved aerosol properties. The physical basis for existing satellite aerosol remote sensing retrievals lies in the single scattering nature of the tenuous atmosphere. Invoking the single scatter approximation, the total reflection of solar radiation may be approximated by [*King et al.*, 1999],

$$R \approx R_a + R_s + R_m, \tag{1}$$

[1]Department of Atmospheric Science, Colorado State University, Fort Collins, Colorado, USA.

0148-0227/07/2007JD008535$09.00

where R_a, R_m and R_s respectively describe the component of reflection due to aerosols, gaseous molecules and the surface. Assuming that both the surface and the molecular reflection can be characterized, the reflection due to aerosol is inferred as a residual. Equation (1) illustrates that a misrepresentation of either the molecular or surface reflection will result in an error in the inferred reflection due to aerosol and as such these assumptions must be considered potential sources of uncertainty. The reflection due to a single scattering aerosol may further be described in terms of the aerosol optical properties as [*King et al.*, 1999],

$$R_a = \frac{\tau_a \omega_a P_a}{4\mu\mu_o}, \tag{2}$$

where τ_a, ω_a and P_a are the aerosol optical depth (AOD), the single scatter albedo and the scattering phase function, while μ and μ_o are the cosines of the viewing and solar zenith angles (SZA). In general the component of the reflection ascribed to aerosol is used to deduce the AOD, which requires the additional assumption of the aerosol scattering and absorption properties (P_a, ω_a) of the aerosol. As with the previous assumptions of the molecular and surface reflection functions, the assumption of aerosol optical properties introduces additional uncertainty in the retrieved AOD estimate.

[4] Numerous algorithms based on the above physical principles have been developed over the last few decades to infer AOD over the global oceans from satellite measurements. For example, pioneering retrievals were performed using single channel radiances from the Advanced Very High Resolution Radiometer (AVHRR) by *Ignatov and Stowe* [2000]. The single channel nature of these retrievals offer no additional information to constrain the assumed aerosol properties, however, retrieved optical depths at two wavelengths may further be used to calculate an Angstrom exponent, which provides an indirect estimate of the particle size. The Moderate Resolution Imaging Spectroradiometer (MODIS) instruments on board NASA's Terra and Aqua satellites [*Tanré et al.*, 1997] offers the added benefit of several high spectral and spatial resolution measurements from the visible through the shortwave infrared. The spectral information improves upon single channel algorithms by constraining the aerosol optical properties outlined in equation (2) allowing the MODIS algorithm to estimate aerosol microphysical properties. With the successful flight of the Multiangle Imaging SpectroRadiometer (MISR) aboard EOS Terra, AOD retrievals based on multiangular measurements of spectral reflectance that sample the aerosol scattering phase function have recently been implemented [*Kahn et al.*, 2005]. The additional constraint on the wavelength-dependent aerosol scattering phase function reduces uncertainty due to assumptions of aerosol size and shape. The Polarization and Directionality of the Earth's Reflectances (POLDER) I, II and III instruments have extended this concept to include spectral measurements of the linear polarization [*Deuzé et al.*, 2000]. The addition of polarization information to multiangular radiance measurements has been shown to further constrain aerosol chemical composition through the real part of the refractive index [*Mishchenko and Travis*, 1997] and provides increased sensitivity to scattering by small aerosol [*Chowdhary et al.*, 2005]. The planned NASA Glory mission [*Mishchenko et al.*, 2007] will carry the Advanced Polarimetry Sensor (APS) that improves upon current aerosol sensing platforms by combining the spectral multiangular and polarization capabilities of all of the aforementioned instruments. Thus satellite observations of aerosol have evolved from highly underdetermined single channel retrievals to multispectral, multiple view angle observations including polarization in an effort to better constrain the optical properties that influence the measurements. Despite the substantial improvement in both the quality and quantity of the observations, critical assumptions of both aerosol and surface characteristics must still be made in order to retrieve aerosol properties. The information content of spectral polarization measurements from a single view angle have been addressed by *Hasekamp and Landgraf* [2005] while *Hasekamp and Landgraf* [2007] have further examined the capabilities of multiple view angles and polarization over land surfaces. However, these works do not address the issue of forward model assumptions such as the surface reflectance and aerosol microphysical model, as a source of retrieval uncertainty. The analysis presented here adds to this work by addressing near-infrared spectral multiple view angle observations of intensity and polarization over ocean and land surfaces while focusing on these assumptions as a source of retrieval uncertainty. This analysis is necessary both in terms of identifying the limitations of current aerosol products as well as planning future observing missions.

[5] To this end, this paper presents an aerosol information content analysis in an effort to assess the uncertainty in retrieved aerosol microphysical properties and identify possible limitations of multiangular polarized radiance measurements for constraining them. Specifically, the ambiguity in aerosol microphysical parameters retrieved using the measurements employed in the POLDER operational over ocean aerosol retrieval algorithm [*Deuzé et al.*, 2000] is examined and a quantification of the effects of this uncertainty on optical depth retrievals is presented. Section 2 outlines the physical models of radiative transfer and aerosol microphysics developed for this study. The signal to noise ratio, a fundamental property that governs the performance of any retrieval regardless of the framework adopted, is examined in section 3 to highlight the angular and scene-dependent nature of the information content of the measurements. Emphasis is placed on considering physical model assumptions as a source measurement uncertainty in a rigorous error characterization. A further analysis is performed using a singular value decomposition (SVD) to objectively quantify the information content of the aerosol single scattering properties, select an optimal set of retrieval parameters for the measurements considered and highlight the nonunique relationship between aerosol microphysical parameters and optical properties. Section 4 then outlines an aerosol retrieval framework and results of a number of synthetic retrievals are presented in section 5 focusing on the retrieval error characterization. Having analyzed the inversion method, retrievals are performed using measurements from the POLDER-III instrument flying aboard PARASOL in section 6. A dark ocean surface is contrasted with a mixed forest surface in section 7 in order to highlight the added benefits of polarization measure-

Table 1. Parameters Defining the Size Distribution and Optical Properties of the a Priori Aerosol Model

Parameter	Accumulation Mode	Coarse Mode
N, m^{-2}	10^{12}	10^{9}
r_e, μm	0.15	2.5
v_e, μm	0.2	0.5
m_r	1.45	1.45
m_i	0.0035	0.0035

ments over land. Finally, section 8 outlines some conclusions and thoughts for extension of this work.

2. Physical Models

[6] Aerosols have been shown [*Davies*, 1974] to follow a multimodal log-normal number size distribution,

$$N(r) = \sum_{i=1}^{n} \frac{N_i}{\sqrt{2\pi}\sigma_i r} \exp\left[\frac{-\left(\ln r - \ln r_{g,i}\right)^2}{2\sigma_i^2}\right]. \quad (3)$$

Here N_i, σ_i and $\ln r_{g,i}$ are the number concentration, standard deviation of the distribution of the natural logs of the rs, and the mean of the distribution of the natural logs of the rs, respectively. Each mode of the size distribution represents a single independent aerosol source and several modes may coexist at any given time in any given place. In principle each mode of the size distribution may represent a unique source and as a result may have a different chemical composition and thus a different value of index of refraction. It has been shown [e.g., *Deuzé et al.*, 2000] that retrieval algorithms that only consider a single aerosol mode suffer from errors due to misrepresented polarization scattering by small aerosols while a bimodal distribution is able to capture the optical properties of the aerosol. Thus a bimodal distribution is adopted here. Throughout the paper, primed quantities will be used to refer to accumulation (small) mode parameters while double primed quantities will refer to the coarse (large) mode.

[7] The parameters defining the base state microphysical model used throughout this work are derived from the climatology of *d'Almeida et al.* [1991] and Aerosol Robotic Network (AERONET) climatology [*Dubovik et al.*, 2002; *Smirnov et al.*, 2002] and are listed in Table 1. The size distribution here is described in terms of the effective radius and effective variance of the two modes defined following *Hansen and Travis* [1974] as,

$$r_{e,i} = r_{g,i} \exp\left(\frac{5}{2}\sigma_i^2\right) \quad (4)$$

$$v_{e,i} = \exp\left(\sigma_i^2\right) - 1. \quad (5)$$

Similarly the effective radius of the total distribution may be derived for a number of log-normal modes as,

$$r_e = \frac{\sum_{i=1}^{n} N_i r_{g,i}^2 \exp\left(\frac{9}{2}\sigma_i^2\right)}{\sum_{i=1}^{n} N_i r_{g,i} \exp\left(2\sigma_i^2\right)} \quad (6)$$

An additional parameter considered here is the logarithm of the ratio of the number concentration of the two modes, $\gamma = \mathrm{Log}_{10}(N'/N'')$, that governs the weighting of the optical properties of the two modes of the size distribution.

[8] Assuming spherical particles, the optical properties of the aerosol distribution are diagnosed using Mie theory for any given set of aerosol microphysical properties, $\mathbf{x} = [\gamma, r_e', r_e'', v_e', v_e'', m_r', m_r'', m_i', m_i'']$, yielding ω_a and a scattering phase matrix containing four unique elements,

$$\mathbf{P}(\Theta) = \begin{pmatrix} P_{11} & P_{12} & 0 & 0 \\ P_{12} & P_{11} & 0 & 0 \\ 0 & 0 & P_{33} & P_{34} \\ 0 & 0 & -P_{34} & P_{33} \end{pmatrix}, \quad (7)$$

where P_{11} is the aerosol scattering phase function and Θ is the scattering angle. Figure 1 shows the phase matrix elements for the base state microphysical model outlined in Table 1. Note that the base state model is a linear combination of the coarse and accumulation mode models and that the weighting between the modes is given by γ. For any combination of aerosol model given by $\mathbf{x}$ and optical depth the aerosol column number concentration may be derived. The calculated aerosol optical properties are input into a radiative transfer model implementing the doubling-adding solution method [*Evans and Stephens*, 1991] to calculate top of the atmosphere (TOA) linearly polarized radiance fields. The model solves the radiative transfer equation through a numerical quadrature discretization in zenith angle and a Fourier discretization in azimuth angle. It has been operated with twenty four quadrature angles per hemisphere while two hundred and fifty six discretely sampled azimuth angles have been used to calculate thirty Fourier modes. The model solves for the truncated Stokes vector $\mathbf{I} = [I, Q, U]^T$ that describes the linear polarization state of the radiance field [*Van de Hulst*, 1981], the quantity measured by the POLDER instrument. This results in the elimination of the last row and column of equation (7) leaving three unique elements describing the angular single scattering properties of the aerosol. On the basis of the POLDER operational products [*Deuzé et al.*, 2000] the

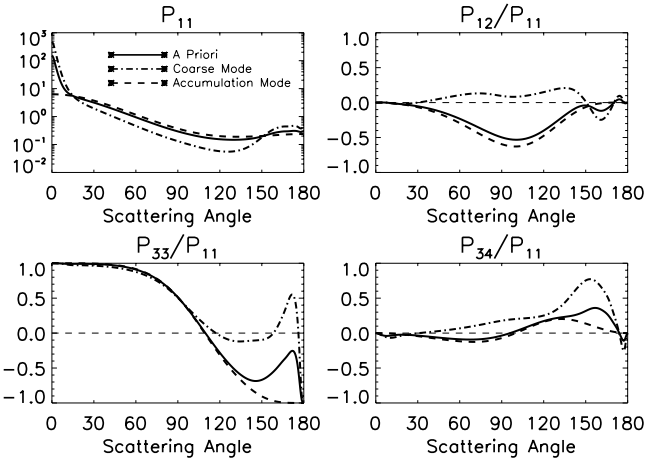

Figure 1. A priori scattering phase matrix elements along with the individual coarse and accumulation mode elements at 670.2 nm.

following normalized dimensionless quantities are considered in this work,

$$I_n = \frac{\pi I}{F} \tag{8}$$

$$q = \frac{Q}{I} \tag{9}$$

$$u = \frac{U}{I} \tag{10}$$

$$L_n = \frac{\pi}{F}\sqrt{Q^2 + U^2}, \tag{11}$$

where F is the top of the atmosphere incident solar flux. Given the single scattering nature of the tenuous atmosphere a single layer model consisting of Rayleigh scattering molecules and aerosols overlying a rough ocean surface is considered. Molecular optical depth is calculated using the parameterization [*Hansen and Travis*, 1974],

$$\tau_R = \frac{p}{p_o} 0.008659\lambda^{-4}\left(1 + 0.0113\lambda^{-2} + 0.00013\lambda^{-4}\right) \tag{12}$$

where p_o = 1013.25 hPa and λ is the wavelength in micrometers, while gaseous absorption is assumed negligible in the wavelengths modeled here. The surface reflection has been prescribed through an implementation of the empirically derived model of *Koepke* [1984]. This model diagnoses a Gaussian wave slope distribution [*Cox and Munk*, 1954] and the fractional coverage of sea foam as a function of wind speed. The optical properties of the sea surface are then calculated as a combination of specular reflection from the waves and isotropic reflection from the foam.

[9] It is important to remember that the calculated radiances are a function of many parameters including the surface reflection, molecular optical depth, the vertical profile of aerosols and all of the nine parameters that define the aerosol microphysical model. Aerosol retrievals using the measurement set considered here require the assumption of many of these parameters and the combined effect of these assumptions on near-infrared satellite aerosol retrievals is a central focus of this study.

3. Information Content and Error Characterization

[10] Before developing any retrieval algorithm it is critical to quantify the information contained in the measurements one seeks to invert. The POLDER instrument makes measurements of the truncated Stokes vector $\mathbf{I} = [I, Q, U]^T$ in three of its nine channels and from twelve to fourteen viewing geometries [*Deschamps et al.*, 1994]. This research focuses on two channels that are commonly used for the remote sensing of aerosols over oceans (670.2, 860.8 nm). Following the POLDER aerosol algorithm the 490 nm channel is not considered because of uncertainty in the water leaving radiances [*Morel*, 1988]. Inclusion of a channel in this region of the visible spectrum would require a model of the light exiting the ocean body such as that of *Chowdhary et al.* [2006]. With measurements of $\mathbf{I} = [I, Q, U]^T$ made at twelve viewing angles in two channels, a total of $3 \times 12 \times 2 = 72$ measurements are considered. This is a large observation set, however, not all of the observations are independent nor do they all provide equal information. In an effort to highlight the information content of the multiangular polarization measurements this section introduces the signal to noise ratio (SNR) as a measure of information that explicitly makes use of a detailed error characterization methodology in the context of an AOD retrieval. A further analysis of the independence of the microphysical signature in the aerosol single scattering properties is subsequently performed using an SVD technique that identifies the number of retrievable microphysical parameters and quantifies the information added by multiangular polarization measurements.

3.1. Signal to Noise Ratio and Error Characterization

[11] To motivate the need for a rigorous error characterization methodology, the measurement SNR is analyzed with respect to an AOD retrieval beginning with a review of the functional dependencies of these measurements. The modeled radiances for any given geometry are a function of both the retrieval parameters as well as the many assumptions which have been made in defining both the aerosol and radiative models. In general, this is expressed mathematically as,

$$\mathbf{y} = \mathbf{F}(\mathbf{x}, \mathbf{b}) + \mathbf{n}, \tag{13}$$

where $\mathbf{y}$ is the measurement vector, $\mathbf{F}$ is the forward radiative transfer model, $\mathbf{x}$ is a vector of the retrieval parameters, $\mathbf{b}$ is a vector of forward model assumptions and $\mathbf{n}$ is a vector of instrument uncertainties. The retrieval problem is an attempt to invert this equation in order to infer the value of $\mathbf{x}$ based on the measurements, $\mathbf{y}$. Considering a linear problem equation (13) may be expressed as [*Rodgers*, 2000],

$$\mathbf{y} = \mathbf{F}(\mathbf{x}_o, \mathbf{b}) + \mathbf{K}(\mathbf{x} - \mathbf{x}_o) + \mathbf{n} \tag{14}$$

$$\mathbf{K} = \frac{\partial \mathbf{F}(\mathbf{x}, \mathbf{b})}{\partial \mathbf{x}}. \tag{15}$$

Equations (14) and (15) demonstrate that our ability to map between the state space, $\mathbf{x}$, and the measurement space, $\mathbf{y}$, is a function of the sensitivity of the measurements to the state parameters, given by $\mathbf{K}$, as well as both instrument uncertainty and any assumptions that are made in order to perform the radiative transfer calculations. Therefore a realistic error estimate must take into account both the instrument measurement uncertainty, $\mathbf{n}$, as well as the natural variability of the assumed parameters in the vector $\mathbf{b}$.

[12] The SNR provides a useful measure of the information contained in a measurement. The signal component of this ratio is given by the matrix $\mathbf{K}$ and is obtained through straightforward evaluation of the radiative transfer model for perturbations to the base state. On the other hand, many sources of error must be taken into account to properly

Table 2. Estimates of the Dynamic Ranges of the Parameters Defining the Physical Models

Parameter	Error Estimate
r_e, μm	
Accumulation mode	±0.05
Coarse mode	±0.5
v_e, μm	
Accumulation mode	±0.1
Coarse mode	±0.3
m_r	
Accumulation mode	±0.1
Coarse mode	±0.1
m_i	
Accumulation mode	±0.0015
Coarse mode	±0.0015
γ	± one order of magnitude
Wind speed	2–20 m/s
Vertical distribution	aerosol scale height = 1.5 *km*
Measurement	5%

estimate the noise component originating from the assumptions contained in the vector **b**. To rigorously quantify the view angle-dependent errors associated with an AOD retrieval, twelve independent sources of error have been considered, nine of which are associated with the aerosol model assumptions while the remaining three are associated with the surface reflection function, the vertical distribution of the aerosol (modeled with an eight layer atmosphere) and the instrument measurement uncertainty. In order to define the errors associated with physical model assumptions, estimates of each parameter's dynamic range, based on a survey of the literature [*Dubovik et al.*, 2002; *Smirnov et al.*, 2002; *d'Almeida et al.*, 1991; *Hagolle et al.*, 1999; *Monahan*, 2006], are outlined in Table 2. Radiative transfer calculations performed at the extremes of these dynamic ranges have been used to estimate an error due to each source. Assuming that distinct sources of error are independent, the total measurement noise in the *i*th measurement is calculated as the square root of the sum of the squares of the individual errors, Δ_{ij}, as follows,

$$\varepsilon_i = \sqrt{\sum_j \Delta_{ij}^2}. \tag{16}$$

These calculations were repeated for 15 different atmospheric scenes composed of five aerosol optical depths and three solar zenith angles. It should be noted that several sources of error have been neglected in Table 2. These include gaseous absorption that is negligible in the channels considered, water leaving radiances and three-dimensional radiative effects that are not handled by the radiative transfer model. Additionally, the effects of aerosol nonsphericity have been handled elsewhere [*Kahn et al.*, 1997; *Gérard et al.*, 2005] and are not considered here. It is further noted that recent work by *Dubovik et al.* [2006] using the AERONET climatology offers a thorough description of the scattering properties of nonspherical aerosol in dusty environments. Finally, potential measurement errors in the degree of linear polarization have not been addressed here. It has been shown [*Mishchenko and Travis*, 1997] that uncertainty in the observed linear polarization may lead to errors in retrieved aerosol parameters that are larger than those required for climate research [*Mishchenko et al.*, 2004].

[13] Figure 2 shows polar maps of sensitivity of the radiance and polarized radiance to AOD, total errors and the ratio of these two quantities, the signal to noise ratio. Recall that the sensitivity is defined as the partial derivative of the normalized intensity and linearly polarized intensity with respect to AOD as calculated by equation (15) and the errors are given by equation (16). Although the signal maps suggest that the largest scattering angles contain the most AOD information, the errors are compounded at these angles as well. The combination of these two pieces of information demonstrate that the view angles that contain the most information in fact form annular structures around the backscatter direction for the intensities and around the sunglint region for the polarization. The minimum in sensitivity of the scalar intensity within the sunglint region offers an opportunity to clarify the definition of signal employed in this work. From a detector standpoint signal is the radiant intensity whereas from a retrieval point of view signal is considered the sensitivity of the radiative transfer model to the retrieval parameters given by equation (15). Within the sunglint the intensity is a maximum (large signal

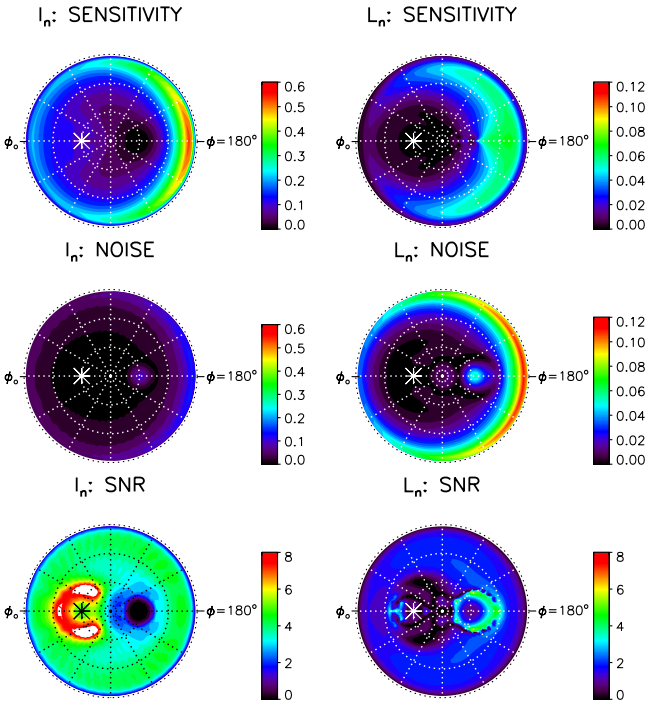

Figure 2. Polar maps of the sensitivity to optical depth, the calculated measurement noise and the signal to noise ratio plotted for both the normalized scalar intensity and the normalized linearly polarized intensity. The sensitivity shown is given by $\frac{\partial \mathbf{F}(\tau)}{\partial \tau}$ while the noise is calculated as $\varepsilon_i(\tau) = \sqrt{\sum_j \Delta_{ij}^2}$ and the SNR is the ratio of these two quantities. Calculations are performed for an aerosol optical depth of 0.2 at 860.8 nm and a solar zenith angle of 30°. The asterisk indicates the position of the Sun and the dashed annular rings represent viewing zenith angles of 30, 60, and 90°.

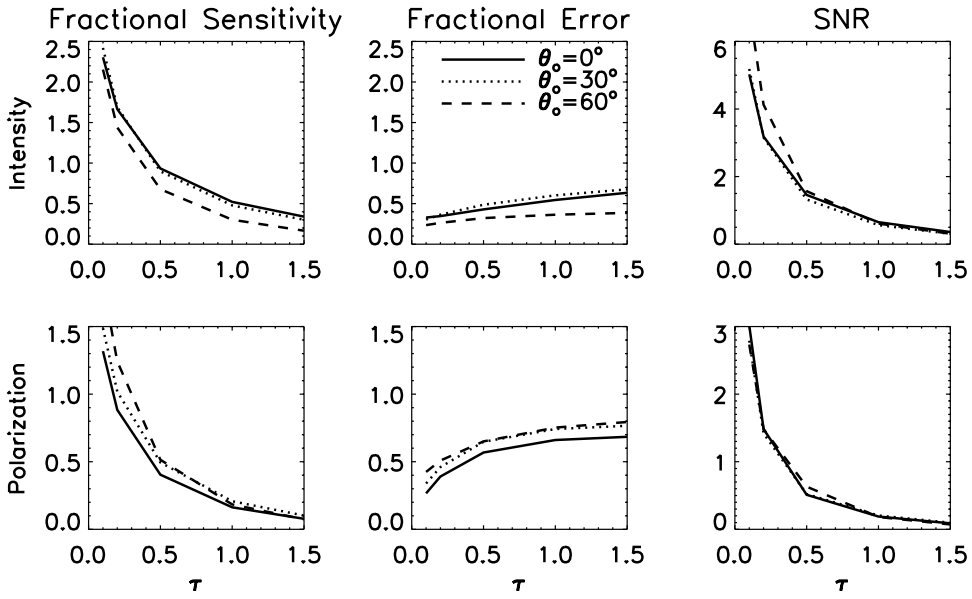

Figure 3. Hemispheric average fractional sensitivity to AOD, total fractional error and SNR of the normalized intensity and linearly polarized intensity at 670.2 nm. The averages are weighted by $\sin(\theta)$ to account for the angular area of each calculated radiance so as not to bias the average toward the near nadir points. For the intensities the fractional sensitivity shown here is given by $\frac{\partial \mathbf{F}(\tau)}{I(\tau)\partial\tau}$, the fractional error is given by $\frac{\varepsilon(\tau)}{I(\tau)}$ and the SNR is given by the ratio of these two quantities. Similar equations apply to the polarization. Note that the fractional errors greatly exceed the assumed 5% instrument uncertainty.

from a detector point of view), however the sensitivity of the forward model to AOD perturbations is a minimum (small signal from a retrieval point of view). The mechanism causing this behavior is that increased AOD increases the atmospheric contribution to the radiance while simultaneously decreasing the large surface contribution to the radiance and these two competing effects approximately balance each other.

[14] It is important to emphasize that both the model sensitivity and total error are a function of scene, that is, both parameters change in magnitude with respect to the AOD. This is demonstrated in Figure 3, which shows the average fractional sensitivity, fractional noise and SNR for three solar zenith angles. The fractional quantities here have been normalized by the intensity and polarized intensity calculated at a given optical depth using equations (8) and (11). First note that the fractional errors in both the normalized intensity and the polarized intensity significantly exceed the 5% assumed measurement uncertainty implying retrieved AOD uncertainty derives primarily from aerosol microphysical and forward model assumptions. It is generally observed that the magnitude of the fractional signal is greater for the intensity than for the polarization and that the SNR is greater for the intensity as well. This implies that most of the information regarding the AOD lies in the intensity measurements as opposed to the polarization. It is also found that measurement sensitivity to AOD decreases with increasing AOD due to saturation of the reflection function while noise increases with increasing AOD due to increasing influence of the aerosol model assumptions on the upwelling radiance. The net result is that the SNR decreases sharply with AOD. The implication is that AOD errors may be compounded at large AOD in the absence of additional constraints on aerosol microphysical properties. Conversely, this implies that microphysical properties may be derived with greater certainty for large optical depths. Figures 2 and 3 together demonstrate that both the signal and the noise are dependent on viewing geometry and AOD, making some measurements preferable to others. The retrieval algorithm outlined below utilizes the results of this analysis in a flexible measurement weighting scheme that accounts for the angular and scene-dependent nature of the errors.

3.2. Microphysical Information Content

[15] Given that aerosol microphysical assumptions are a source of uncertainty for AOD retrievals it is desirable to use the observations to constrain the microphysics in order to reduce those errors. Because of the uncertainties and inherent correlations between channels, however, it is not obvious how many parameters can be constrained using any given set of observations. It is therefore important to quantify the number of independent pieces of information that may be derived from various combinations of the spectral, angular and polarization measurements of the POLDER instrument. The analysis method used here assumes that the phase matrix elements are fully sampled for scattering angles greater than 60°. In order to examine the information content of the angular and polarized radiances at these two channels we introduce a matrix of model sensitivities of the form,

$$\mathbf{S} = \mathbf{x}^T \frac{\partial \tilde{\mathbf{P}}(\Theta)}{\partial \mathbf{x}}, \tag{17}$$

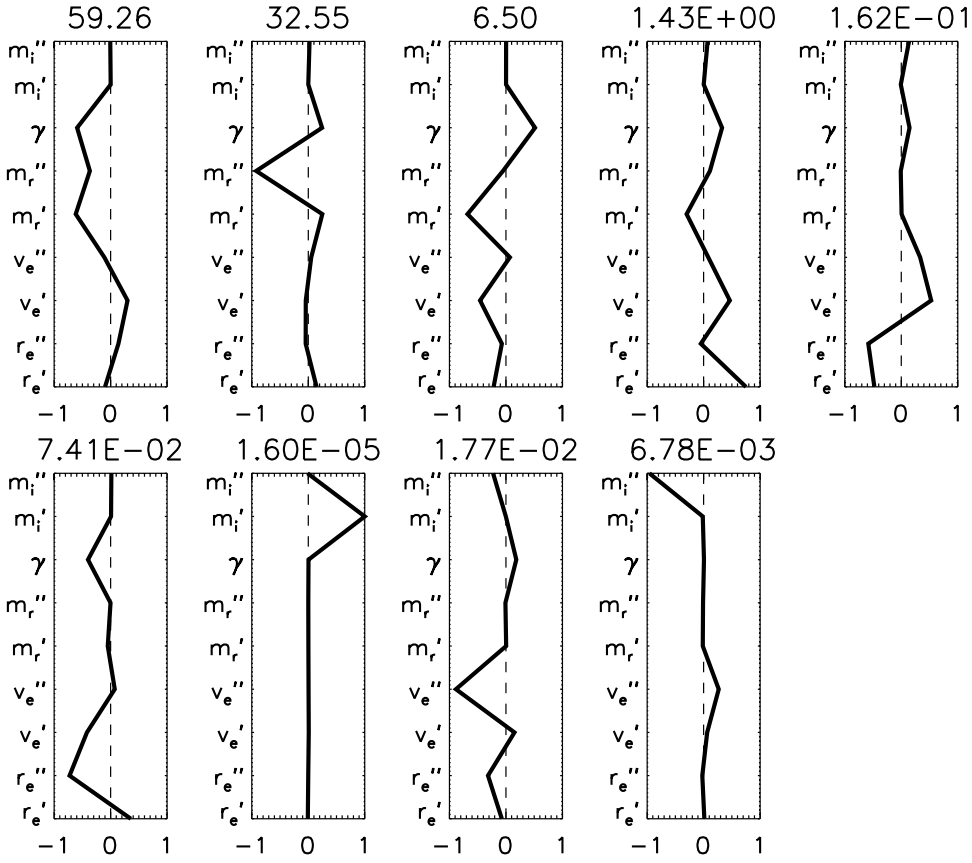

Figure 4. Singular vectors of the sensitivity covariance matrix along with the percent variance explained by each individual vector.

where $\tilde{\mathbf{P}}(\Theta) = \left[[P_{11}, \frac{P_{21}}{P_{11}}, \frac{P_{33}}{P_{11}}]_{670}, [P_{11}, \frac{P_{21}}{P_{11}}, \frac{P_{33}}{P_{11}}]_{860}\right]$ and $\mathbf{x} = [\gamma, r_e', r_e'', v_e', v_e'', m_r', m_r'', m_i', m_i'']$. Each of the 6 phase matrix elements in **P** are sampled in half degree scattering angle increments from 60 through 180° resulting in $6 \times 241 = 1446$ samples of the aerosol single scattered radiation field. The vector **x** is composed of 9 microphysical quantities that define the phase matrix. Thus **S** is a matrix of dimensions 1446×9 representing the change in each phase matrix element at each wavelength and scattering angle given a fractional change in each microphysical parameter that defines the aerosol model. The matrix **S**, therefore, captures the spectral, angular and polarization state of single scattered radiation at the wavelengths considered here. For a given optical depth and single scattering albedo it is these single scattering properties that govern the atmospheric radiative transfer and therefore any limitations identified in the aerosol single scattering properties will propagate into a spaceborne retrieval using models of radiative transfer.

[16] In order to identify and quantify the number of retrievable microphysical parameters a singular value decomposition (SVD) is utilized. The matrix **S** is decomposed as,

$$\mathbf{S} = \mathbf{U}\Lambda\mathbf{V}^T, \tag{18}$$

where Λ is a diagonal matrix of singular values (λ). It follows that,

$$\mathbf{S}^T\mathbf{S} = \mathbf{V}\Lambda^2\mathbf{V}^T, \tag{19}$$

is a covariance matrix of the sensitivities of the spectral phase matrix elements to the aerosol microphysical parameters. The Eigenvectors are interpreted as linearly independent combinations of the measurements that reproduce some fraction of the variance of $\mathbf{S}^T\mathbf{S}$ and the fraction of variance explained by the jth Eigenvector is given by $\frac{\lambda_j^2}{\sum_i \lambda_i^2}$ where λ_j^2 is the corresponding Eigenvalue. Additionally, the spectrum of the Eigenvalues quantify the number of unique parameters needed to reproduce the sensitivity covariance. The broader the spectrum, the larger the number of microphysical parameters necessary to reproduce the covariance implying that a greater number of parameters may be retrieved from the observations.

3.2.1. Number of Retrievable Quantities

[17] The sensitivity of $\tilde{\mathbf{P}}(\Theta)$ has been analyzed about the base state aerosol model described in Table 1 using the SVD. Each of the nine Eigenvectors is plotted in Figure 4 along with its corresponding percent variance explained. Of immediate note is that the first Eigenvector explains nearly 60% of the variance and that this vector is dominated by the real part of the index of refraction of both modes and γ implying that m_r and γ explain the majority of the sensitivity variance. The second singular vector explains an additional 32% of the variance and is dominated by the same parameters. The fact that the majority of the eigenvectors demonstrate multiple peaks is an indication of correlated or nonunique sensitivities of the angular scattering properties to these parameters. The implication is that

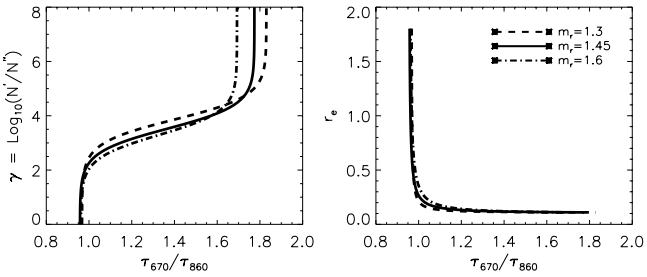

Figure 5. Theoretical relationships for three indices of refraction between the ratio of the spectral optical depths and both γ and the effective radius.

fewer than the full set of nine parameters are required to reproduce the requisite optical properties. The remaining seven Eigenvectors explain roughly 8% of the variance suggesting that it may be possible to constrain one additional parameter from observations of the spectral scattering phase matrix, however, these vectors continue to exhibit multiple peaks indicating additional correlated sensitivities to the microphysical parameters. The net effect of the correlations highlighted in Figure 4 is that the combination of microphysical quantities required to reproduce the aerosol single scattering properties in not unique.

[18] This analysis considers error free sampling of the aerosol scattering matrix through a full 120° of scattering angle. Near-infrared spectral, multiangular, and polarization characteristics of the aerosol optical properties are considered simultaneously. Therefore the results represent an upper bound on the information content of observations of these aerosol optical properties to constrain aerosol microphysical properties. It follows that at most three microphysical parameters can be constrained from the measurement set utilized by the POLDER operational over ocean aerosol algorithm. The results further suggest that aerosol optical properties are most sensitive to the real part of the index of refraction as has been suggested by previous work [*Mishchenko et al.*, 1997] and the parameter γ, that provides a measure of particle size that is directly tied to the aerosol microphysics and is indicated in nearly all of the Eigenvectors shown in Figure 4. Equivalently, the total effective radius of the distribution could be chosen to represent particle size, however, as can be seen in equation (6), the effective radius of a the bimodal distribution is a nonunique function of five microphysical parameters. In addition, Figure 5 demonstrates that for a given microphysical model γ can be conveniently related to the ratio of the spectral optical depths, whereas the relationship between the equivalent effective radius and spectral AOD ratio demonstrates two distinct regimes with very little transition region between these regimes. The choice of m_r and γ as the ideal retrieval parameters seems intuitive in that these two parameters are respectively able to account for variability in aerosol composition and size.

3.2.2. Spectral Versus Multiangular and Polarization Information Content

[19] To place these results into the historical context of the evolution of aerosol sensing platforms it is of interest to quantify the amount of unique microphysical information contained in each element of the spectral, multiangular and polarization single scattering properties separately. To facilitate this comparison, the previous analysis is repeated twice. Once for a data set containing only the scalar intensity phase matrix elements $[[P_{11}]_{670}, [P_{11}]_{860}]$ and subsequently using only a single view angle at each channel. The result is a spectrum of potentially observable single scattering properties ranging from spectral single view angle intensity sampling to spectral multiangle intensity fields, and finally spectral multiangular polarization fields. Comparing the spectra of the fractional variance explained for these three cases provides a basis for determining the relative contribution of each aspect of the measurement (spectral, multiangular, polarization). Figure 6 illustrates the progression of these spectra from one that is sharply peaked at the first eigenvalue for the single view angle observations to broader spectra as the multiangular and finally the polarization information is added. The number of uniquely retrievable quantities increases with each additional element of the observations. This analysis corroborates an analysis by *Tanré et al.* [1996] using a similar technique that found that one microphysical parameter explained over 99% of the variance in spectral measurements of MODIS. Here it is observed that the addition of multiangular (e.g., MISR) information adds a second uniquely retrievable parameter while polarization (e.g., POLDER) adds a third.

[20] Therefore observational platforms with both multiangular and polarization capabilities will offer improved microphysical retrievals and the improved constraint on aerosol microphysical assumptions should in turn reduce the uncertainty in AOD highlighted in section 3.1. Nonetheless, correlations between the sensitivity of the aerosol single scattering properties to microphysical parameters introduce a level of ambiguity in choosing the ideal retrieval parameters. Finally, it should be noted that while a look up table type retrieval may be capable of providing estimates of all of the parameters given in **x**, essentially characterizing the entire microphysical model, these estimates may only be weakly constrained because of the nonunique relationships between the aerosol optical properties and microphysical parameters that define them.

4. Retrieval Methodology

[21] The physical models described in section 2 along with the error characterization of section 3 form the basis for

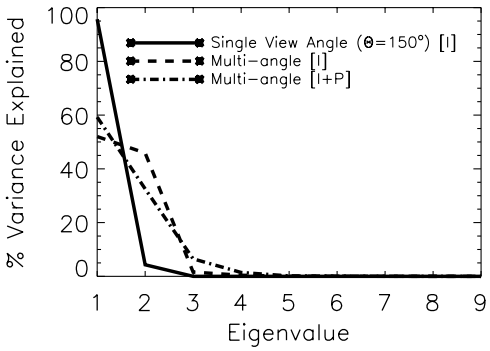

Figure 6. Spectra of the percent variance explained. The three curves correspond to a single view angle intensity measurement (i.e., MODIS), multiangular intensity measurements (i.e., MISR) and multiangular intensity plus polarization measurements (i.e., POLDER).

an aerosol microphysical retrieval introduced here for estimating the spectral AOD along with the aerosol microphysical parameters γ and m_r. The method is formulated for observations from the POLDER-III instrument aboard PARASOL, however it is flexible with regards to the measurement input as well as the retrieval parameters. The weighted least squares retrieval minimizes the cost function,

$$\Phi = [\mathbf{y} - \mathbf{F}(\mathbf{x})]^T \mathbf{S}_y^{-1} [\mathbf{y} - \mathbf{F}(\mathbf{x})], \tag{20}$$

where $\mathbf{y}$ is a vector of measurements and $\mathbf{x}$ is a vector of the retrieved quantities. The matrix, $\mathbf{S}_y$, is the measurement error covariance matrix whose diagonal elements are calculated using the method described in section 3.1 and are allowed to vary as a function of viewing geometry as well as AOD. By only including diagonal elements in $\mathbf{S}_y$ correlated errors have been implicitly ignored. As has been demonstrated in section 3.2, microphysical model assumption errors are correlated and therefore this approximation will tend to slightly overestimate retrieval error offering a useful upper bound on the uncertainty. Linearizing the radiative transfer model about the present state, the cost function is minimized using Newton's method, leading to the following iterative solution for the state vector,

$$\mathbf{x}_{i+1} = \mathbf{x}_i + \left(\mathbf{K}_i^T \mathbf{S}_y^{-1} \mathbf{K}_i\right)^{-1} \mathbf{K}_i^T \mathbf{S}_y^{-1} [\mathbf{y} - \mathbf{F}(\mathbf{x}_i)], \tag{21}$$

where $\mathbf{K}_i = \frac{\partial \mathbf{F}(\mathbf{x}_i)}{\partial \mathbf{x}}$. By further making the assumption of Gaussian error statistics a retrieval error covariance matrix may be derived,

$$\mathbf{S}_x = \left(\mathbf{K}_i^T \mathbf{S}_y^{-1} \mathbf{K}_i\right)^{-1}. \tag{22}$$

Therefore the retrieval produces not only a most likely value $\hat{\mathbf{x}}$, but rather a PDF of the a posteriori knowledge of the state. Both $\mathbf{K}$ and $\mathbf{S}_y$ vary with $\mathbf{x}$, so $\mathbf{S}_x$ provides a dynamic estimate of retrieval uncertainty. The retrieval is considered to have converged when,

$$[\mathbf{x}_{i+1} - \mathbf{x}_i]^T \mathbf{S}_x^{-1} [\mathbf{x}_{i+1} - \mathbf{x}_i] \ll m, \tag{23}$$

where m is the number of degrees of freedom in the retrieval space. An additional retrieval diagnostic is given by the convergent value of the cost function. This is the χ^2 statistic [*Rodgers*, 2000],

$$\chi^2 = [\mathbf{y} - \mathbf{F}(\hat{\mathbf{x}})]^T \mathbf{S}_y^{-1} [\mathbf{y} - \mathbf{F}(\hat{\mathbf{x}})]. \tag{24}$$

Large values of χ^2 indicate poor physical model assumptions in that the radiative transfer model was not well able to match the measurements, to within the accuracy prescribed by $\mathbf{S}_y$. Another useful diagnostic is given by the Shannon Information Content (SIC) [*Rodgers*, 2000],

$$H = -\frac{1}{2} \log_2 |\mathbf{S}_x| \tag{25}$$

that provides a measure of the amount of information added by the measurements relative to a reference state. H may be interpreted as bits of information so that for any given retrieval with a value of H, 2^H states can be distinguished relative to the reference state.

[22] Application of the above theory is performed in two steps. In the first step the spectral AOD is determined along with γ from the intensity measurements only. Equation (21) is applied to the AODs while γ is updated at the end of each iteration based on the curves outlined in Figure 5. For this step y has a length of $2 \times 12 = 24$ while $\mathbf{x} = [\tau_{670}, \tau_{860}]$. Both x and γ are required to reach convergence criterion given by equation (23) and an error estimate is placed on γ through use of standard propagation of the AOD errors. This method permits the retrieval of γ in a manner that is consistent with the spectral behavior of optical depth while decreasing the dimensionality of the retrieval state space and allowing a degree of freedom in the aerosol microphysical assumptions. The second step adds the polarization measurements in order to estimate m_r while holding the other parameters fixed. In this step $\mathbf{y}$ is of length $2 \times 3 \times 12 = 72$ and $\mathbf{x} = [m_r]$.

5. Simulated Retrieval Results

[23] A critical step in evaluating the functionality of a retrieval method is to apply simulated radiances created from data in which the true state is prescribed and thus known exactly. Therefore a simulated measurement data set corresponding to different combinations of POLDER viewing geometries, including both backscattering and sunglint viewing angles, has been created to highlight some potential limitations of aerosol microphysical retrievals utilizing multiangular polarization measurements at near-infrared wavelengths. The atmospheric conditions used to simulate these data sets have been selected using random perturbations of all of the parameters defining the base state physical models within the dynamic ranges outlined in Table 2. It is emphasized that this measurement data set is designed to provide a strenuous test of the retrieval with realistic errors originating from both aerosol microphysical and radiative model assumptions along with a Gaussian instrument uncertainty. Retrieval results are presented in Figure 7.

5.1. AOD

[24] The retrieved AOD correlates well with the true AOD with a correlation coefficient of 0.97 demonstrating that multiangular intensity measurements along with one free microphysical parameter are able to constrain the optical depth. Further justification for using intensity observations only to constrain the AOD is presented in Table 3, which presents an analysis of the SIC for an optical depth retrieval using various combinations of the measurements. A diminishing rate of return is evident with each additional measurement added. It appears that most of the AOD information has been extracted with twelve intensity measurements and that polarization adds only a minor refinement of this parameter, confirming the analysis presented in section 3.

5.2. Ratio of the Bimodal Number Concentrations (γ)

[25] Figure 7 (right) shows a comparison of the retrieved with the true γ with correlation coefficient, $r = 0.66$. The retrieved values tend to track the true values fairly well between two and four but outside of these bounds the

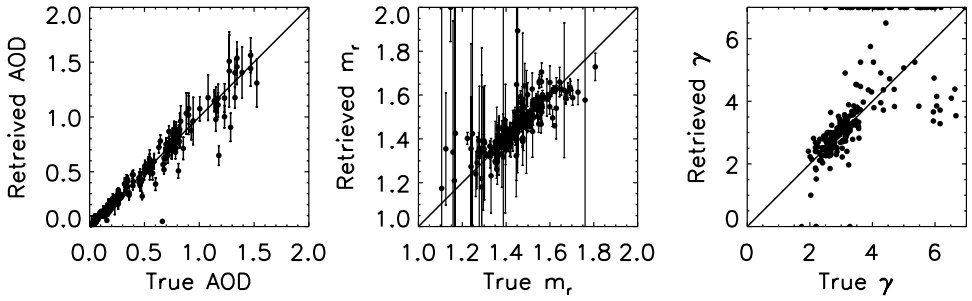

Figure 7. Comparison of the synthetic retrieval result to the prescribed true values used to generate the synthetic data.

correlation is substantially reduced. This behavior is consistent with the theoretical relationships plotted in Figure 5. The aerosol optical properties are essentially insensitive to changes in γ outside of this range and are able to take on multiple values and still match the measurements. Note, however, that the two limits represent very distinct conditions. A value of $\gamma > 4$ is indicative of an air mass dominated by accumulation mode aerosol whereas $\gamma < 2$ indicates a significant presence of coarse mode particles. The parameter γ then provides a rough yet useful index of the size of the aerosol of value for many applications.

5.3. Refractive Index (m_r)

[26] Figure 7 (middle) shows comparisons of the retrieved index of refraction with the true values. It is emphasized that this must be considered an effective refractive index as it is not necessarily true that both modes of the size distribution or even all of the particles within a single mode will have similar composition and therefore may have different refractive indices. Good agreement is observed with the retrieved values correlating with the true values at $r = 0.7$, although some notable outliers occur on occasion.

5.4. Error Analysis

[27] As has been outlined in sections 3 and 4, the retrieval produces a dynamic uncertainty estimate that is a function of the retrieval state. Error estimates along with the actual errors of the retrievals are displayed in Figure 8. Encouragingly, the dynamic uncertainty estimates track well with the actual retrieval errors demonstrating a similar functional dependence on the AOD. Optical depth, m_r and γ are generally constrained to within roughly 15%, 5%, and one order of magnitude respectively with the exception of pristine environments with AODs below 0.1 where uncertainty estimates approach 100% for the AOD and index of refraction and several orders of magnitude for γ. The optical depth dependence is less evident for uncertainty in γ because the error associated with this parameter is a strong function of its own value as well as AOD, which highlights the utility of the dynamic uncertainty estimate given by equation (22).

[28] The dynamic nature of the uncertainty estimate presented here is able to capture physics that cannot be explained by a static estimate of uncertainty complicating comparisons with other uncertainty estimates. Nonetheless, an attempt was made to compare the results of this error analysis with those of previous researchers. The AOD uncertainty estimates presented here are generally consistent with previous research, being smaller than those of the AOD-dependent MODIS estimates [*Tanré et al.*, 1997] and comparable with the static estimate of *Mishchenko and Travis* [1997] for single channel polarimetric retrievals. However, the uncertainty in the index of refraction presented here is much larger than the roughly 1% uncertainty quoted by *Mishchenko and Travis* [1997]. No estimates of the γ parameter exist in the literature, however these findings are physically consistent with those of *Mishchenko et al.* [2005] who demonstrated the large uncertainty in estimating aerosol number concentration based on the large sensitivity of this parameter to the effective radius of the size distribution.

Table 3. Average Shannon Information Content (H) for AOD Retrievals Using Various Measurement Sets[a]

Measurement Set	H
1 view angle, intensity	7.25
6 view angles, intensity	9.62
12 view angles, intensity	11.08
12 view angles, intensity/polarization	11.98

[a]Note the diminishing rate of return as measurements are added to the AOD retrieval.

5.5. Examples of Phase Matrix Adjustment

[29] Two specific retrievals have been selected to highlight the ability of the retrieval to match the true aerosol optical properties given two microphysical degrees of

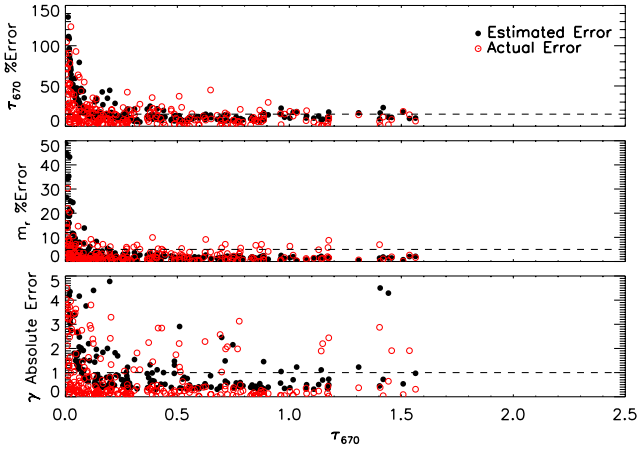

Figure 8. Comparison of the functional dependence of both the retrieval error estimates and the actual retrieval error. (top and middle) Percent errors and (bottom) an absolute error.

Table 4. Example Retrieval Results

Example	γ True	γ Retrieved	m_r True	m_r Retrieved	τ_{670} True	τ_{670} Retrieved
1	6.19	8	1.56	1.56	0.095	0.093
2	2.72	2.92	1.65	1.69	1.70	1.70

freedom (γ, m_r). Retrieval results for the two selected cases are listed in Table 4 and illustrations of the phase matrix elements are shown in Figure 9. These two particular cases were chosen because they represent two extremes, one dominated by the accumulation mode and one dominated by the coarse mode. The phase matrix illustrations elucidate the fact that the retrievals are indeed able to match the true optical properties. After the retrieval second step there is very little difference remaining between the true phase matrix elements and the retrieved. Recall that the aerosol microphysical model used to simulate these measurements was created from random perturbations to all of the microphysical parameters given in Table 1 and that these parameters are held fixed during the retrieval with the exception of γ and m_r. This is another manifestation of the nonuniqueness previously highlighted between the aerosol microphysics and optical properties as it is seen that only γ and m_r are required to reproduce the necessary optical properties. Further examination of Figure 9 demonstrates the utility of m_r in matching the angular aerosol optical properties, particularly in the case of example two. In this case, the sharp peak in the backscattering phase function is only matched after step II through the unique sensitivity of the aerosol optical properties to the index of refraction.

6. Retrievals Using PARASOL Data

[30] Having analyzed the inversion performance using simulated data sets, the retrieval is applied to real data in order to demonstrate that it produces physically plausible results, lending credence to the preceding analysis. For this purpose we examine a substantial dust storm in the Yellow Sea off the coast of China occurring on 17 April 2006 that happened to be the worst dust storm in Beijing in more than five years. Figure 10 shows comparisons of the POLDER operational products with those derived from the present method. The products derived here are plotted on the pixel scale (6×6 km^2) whereas the POLDER products are displayed on the averaged superpixel scale (20×20 km^2). All of the products demonstrate qualitatively good spatial agreement. Of particular interest, the POLDER r_e and γ show the expected anticorrelation. Focusing on the nonglint (east) side of the orbit the retrieved refractive indices demonstrate a qualitatively similar north to south gradient, however, this comparison is confounded by the fact that the POLDER product is only allowed to take on three distinct values. In addition the present retrieval does not include a dust scattering model and the POLDER instrument is sensitive to the optical properties of large nonspherical dust [*Gérard et al.*, 2005] which caused difficulties for the retrieval in matching the observations. In particular, notice the large gray shaded areas represented nonconvergent and

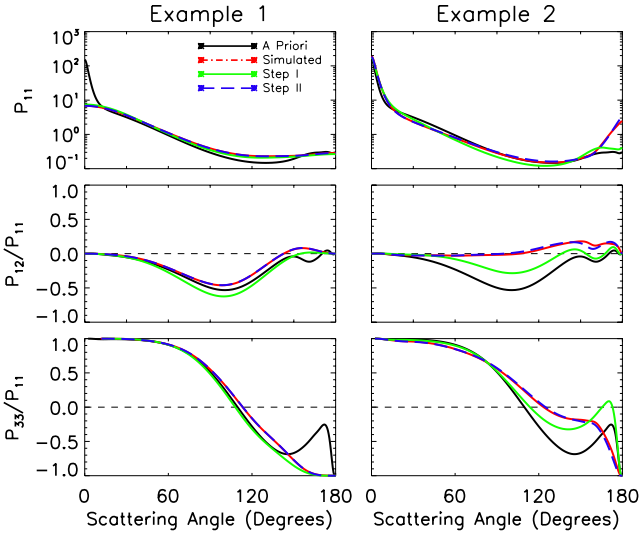

Figure 9. Examples of adjustment of the scattering phase matrix elements for two retrievals. The retrieval begins with the a priori phase matrix and is modified in step I and then step II. Note that only minor differences exist between the simulated (true) phase matrix and that produced by the retrieval. This result affirms that a broad range of optical properties may be simulated with only two free microphysical parameters (γ, m_r).

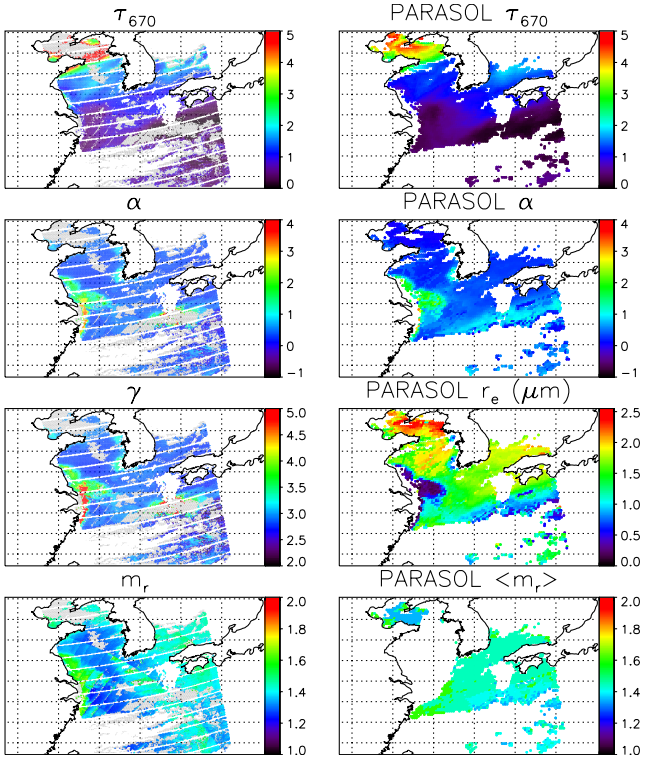

Figure 10. Comparison of the retrieval presented here with the POLDER operational products for a region in the South China Sea. The grey regions indicate postretrieval screened areas. Qualitatively good comparison is seen between the two products demonstrating a physical consistency in the analysis presented here.

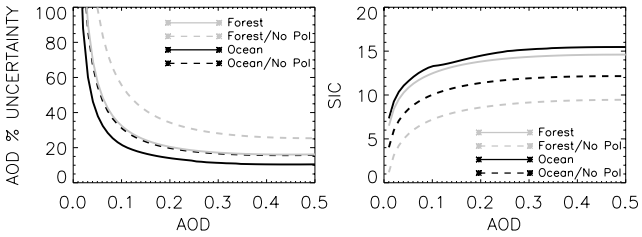

Figure 11. AOD retrieval error and Shannon information content for retrievals over ocean and a mixed forest surface type. Dashed/solid lines are for retrievals that do not/do include polarization measurements.

postretrieval screened data in the northwest and southwest corners of the plots. These pixels were unable to converge because of misrepresented physics, scattering by optically thick dust in the northwest and scattering by cloudy pixels that escaped prescreening in the southeast, that cause the retrieval to reach unphysical or nonconvergent values. While inconvenient at first glance, this behavior is actually positive in that it effectively acts as a screen for cases where algorithm physics is inappropriate for the screening observed such as cloudy and highly nonspherical aerosol cases.

7. Comparison of Land and Ocean Retrievals

[31] The previous retrieval results are applicable to a dark ocean surface. It is worthwhile to compare these results with retrievals over a bright land surface to quantify the relative difference in information provided by retrievals over the two surface types. To facilitate such a comparison a simple model of radiative transfer is employed in which multiple scattering is neglected. Under this approximation, the top of the atmosphere radiance and polarized radiance are given by

$$I = I_{surf} + I_{atm}, \tag{26}$$

$$L = L_{surf} + L_{atm}, \tag{27}$$

where I_{atm} and L_{atm} are the atmospheric scattering terms,

$$I_{atm} = \frac{\omega_a F_o P_{atm}}{4\pi\mu m}(1 - e^{-\tau m}), \tag{28}$$

$$L_{atm} = \frac{\omega_a F_o P_{atm,p}}{4\pi\mu m}(1 - e^{-\tau m}), \tag{29}$$

and I_{surf} and L_{surf} are the surface scattering terms,

$$I_{surf} = \rho\frac{F_o\mu_o}{\pi}(e^{-\tau m}), \tag{30}$$

$$L_{surf} = R_p\frac{F_o\mu_o}{\pi}(e^{-\tau m}). \tag{31}$$

Here R_p is the wavelength-independent polarized fraction of the surface reflectance ρ is the bidirectional reflection function, P_{atm} and $P_{atm,p}$ are the atmospheric phase function and linear polarization phase function, and $m = \frac{1}{\mu} + \frac{1}{\mu_o}$ is the air mass factor. For the following comparison the ocean surface reflection properties are modeled using the ocean surface model outlined in section 2. For land surface reflection, a Lambertian reflecting surface is assumed, in which case, $\rho = \alpha$, the albedo and the angular-dependent polarized reflection is modeled using the empirical model of *Nadal and Bréon* [1999],

$$R_p = \rho_o\left[1 - \exp\left(-\beta\frac{F_p}{\mu + \mu_o}\right)\right]. \tag{32}$$

In this model ρ_o and β are two parameters that depend on the International Geosphere-Biosphere Programme (IGBP) surface classification and the normalized difference vegetation index (NDVI) and F_p is the polarized fraction of the Fresnel reflection.

[32] A mixed forest IGBP surface classification with NDVI > 0.3 is chosen to compare with the ocean surface. Following *Moody et al.* [2005], the surface albedo is prescribed as 0.065 at 670.2 nm and 0.23 at 860.8 nm. Radiances and polarization are modeled for a solar incidence angle of 30° and 12 equally spaced angles in the solar plane from 0 to 55° in zenith angle centered on the nadir view. The base state aerosol microphysical model given in Table 1 is used to calculate the aerosol scattering properties.

[33] The analysis considers the error and information characteristics of retrievals over the two surface types. The retrieval parameters considered follow from the microphysical information content analysis of section 3 as $x = [\tau, \gamma, m_r]$. Equation (22) is used to estimate retrieval errors for a number of different AODs and this error estimate is subsequently used to calculate the SIC. The measurement error covariance matrices are constructed using identical microphysical errors for each surface but with different surface error components. The ocean surface error is taken from the previous analysis whereas the land surface albedo error is estimated from *Moody et al.* [2004] to be 0.03 at 670.2 nm and 0.05 at 860.8 nm.

[34] Results of the analysis are highlighted in Figure 11 for retrievals using intensity only and retrievals using both intensity and polarization measurements. For retrievals utilizing polarization observations, AOD retrieval error is generally about 50% larger over the mixed forest surface than over the ocean. Furthermore, the addition of polarization measurements is shown to reduce errors, particularly for the mixed forest surface type. In the best case scenario at large AOD, without polarization observations, mixed forest retrievals may expect error on the order of 25%. The addition of Polarization reduces this error to 15%. Similar conclusions may be drawn by examining the SIC of the retrievals. This quantity represents the resolution power of each retrieval in terms of bits. Ocean retrievals including polarization provide approximately 1 bit of information more than mixed forest retrievals, implying that roughly twice as much information is available for retrievals over ocean surfaces. When polarization is not included in the analysis the difference in information content is increased to 3 bits meaning that the resolving power of the ocean retrievals is eight times the forest retrievals. The implication is that polarization adds about four times as much

information to the land retrieval than it does to the ocean retrieval. These results highlight the important role for polarization observations in retrievals over land not only in constraining microphysical properties but also in substantial reducing error in the retrieved AOD. This is in contrast to the role that polarization plays over oceans, where it primarily adds information with regards to aerosol microphysical properties.

8. Conclusions

[35] An aerosol information content analysis of the near-infrared measurements utilized in the POLDER over ocean retrieval aerosol retrieval algorithm has been presented. The results demonstrate that the majority of the aerosol optical depth (AOD) information lies in the intensity measurements over oceans. In contrast, it was shown that polarization measurements provide significant AOD information over a mixed forest surface type. Furthermore, it is demonstrated that aerosol microphysical parameters should be retrieved simultaneously with AOD in order to reduce errors. However, a nonunique combination of aerosol microphysical parameters are able to reproduce the same aerosol optical properties. The two polarization sensitive near-infrared channels used in the operational POLDER over ocean aerosol retrieval algorithm are found to be capable of constraining three distinct microphysical parameters offering additional information relative to purely spectral and multiangular sensing techniques. The two most important parameters necessary for simulating the aerosol optical properties at these wavelengths are the real part of the index of refraction (m_r), which demonstrates a unique signature in the polarization measurements, and the logarithm of the ratio of the number concentration of two modes of the size distribution (γ), providing an indication of particle size.

[36] These results were further explored using a novel retrieval for the spectral AOD along with γ and m_r that provides a framework for weighting measurements based on rigorous error estimates of uncertainties deriving from physical model assumptions. The retrieval framework has the advantage of providing several output diagnostics, including a dynamic retrieval error estimate. Through a combination of the diagnostics, some limitations of the measurements were assessed through a number of synthetic retrieval experiments. It was shown, for example, that errors in the ratio of the number concentrations, m_r and AOD are roughly one order of magnitude, 5% and 15%, respectively. An exception occurs in pristine environments with AODs less than 0.1 where these uncertainties approach several orders of magnitude for the number concentration ratio and 100% for both m_r and AOD. Additionally, errors increased by roughly 50% over an IGBP mixed forest surface type. It must be emphasized that these are not retrieval algorithm specific findings but rather they result from a lack of uniqueness in the relationship between the aerosol near-infrared optical properties and the microphysical parameters which define those properties and this may well represent a limitation on the resolving power of current spaceborne observing systems. The advantage of the retrieval framework outlined here is that it provides a dynamic uncertainty estimate that allow for the identification of suspect retrievals on a pixel by pixel basis.

[37] These results further suggest that future retrievals may be substantially improved by adding information from different sensors, another advantage afforded by the retrieval presented here that offers a flexible framework under which both the measurements and the retrieval parameters may vary. NASA's A-train constellation of satellites [*Stephens et al.*, 2002] provides an ideal platform for such synergistic retrieval approaches. The recently launched CALIPSO LIDAR and the planned Orbiting Carbon Observatory (OCO) [*Crisp et al.*, 2004] satellites, for example, respectively offer the potential to further constrain aerosol vertical distributions and absorption properties through vertically resolved backscatter measurements and high spectral resolution measurements in the Oxygen A-Band. Additionally, the NASA Glory mission [*Mishchenko et al.*, 2007] will carry the APS instrument that improves upon the measurement capabilities of POLDER through its enhanced spectral range, increased number of view angles and greater accuracy of polarization observations. Seamless integration of the information provided by these various platforms through a framework that includes appropriate error weighting like that presented here will be a critical component in future attempts to characterize aerosol properties on a global scale.

[38] **Acknowledgments.** This research was supported through the Ball Aerospace–Colorado State University Joint Research Program/Fellowship under agreement PO-03DLB10045 and NOAA grant NA17RJ1228. The authors wish to thank Laurent Labonnote for supplying the PARASOL radiances and data products used in this study.

References

Albrecht, B. (1989), Aerosols, cloud microphysics, and fractional cloudiness, *Science*, *245*, 1227–1230.

Chowdhary, J., B. Cairns, M. I. Mishchenko, P. V. Hobbs, G. F. Cota, J. Redemann, K. Rutledge, B. N. Holben, and E. Russel (2005), Retrieval of aerosol scattering and Absorption properties from photopolarimetric observations over the ocean during the CLAMS Experiment, *J. Atmos. Sci.*, *62*, 1093–1117.

Chowdhary, J., B. Cairns, and L. D. Travis (2006), Contribution of water-leaving radiances to multiangle, multispectral polarimetric observations over the open ocean: Bio-optical model results for case 1 waters, *Appl. Opt.*, *45*, 5542–5567.

Cox, C., and W. Munk (1954), Measurement of the roughness of the sea surface from photographs of the Sun's glitter, *J. Opt. Soc. Am.*, *44*, 838–850.

Crisp, D., et al. (2004), The Orbiting Carbon Observatory (OCO) Mission, *Adv. Space Res.*, *34*, 700–709.

d'Almeida, G., P. Koepke, and E. Shettle (1991), *Atmospheric Aerosols: Global Climatology and Radiative Characteristics*, A. Deepak, Hampton, Va.

Davies, C. N. (1974), Size distribution of atmospheric particles, *J. Aerosol Sci.*, *5*, 293–300.

Deschamps, P. Y., F. M. Bréon, M. Leroy, A. Podaire, A. Bricaud, J. C. Buriez, and G. Seze (1994), The POLDER mission: Instrument characteristics and scientific objectives, *IEEE Trans. Geosci. Remote Sens.*, *32*, 598–615.

Deuzé, J. L., P. Goloub, M. Herman, A. Marchand, and G. Perry (2000), Estimate of the aerosol properties over the ocean with POLDER, *J. Geophys. Res.*, *105*, 15,329–15,346.

Dubovik, O., B. N. Holben, T. F. Eck, A. Smirnov, Y. J. Kaufman, M. D. King, D. Tanré, and I. Slutsker (2002), Variability of absorption and optical properties of key aerosol types observed in worldwide locations, *J. Atmos. Sci.*, *59*, 590–608.

Dubovik, O., et al. (2006), Application of spheroid models to account for aerosol particle nonsphericity in remote sensing of desert dust, *J. Geophys. Res.*, *111*, D11208, doi:10.1029/2005JD006619.

Evans, K. F., and G. L. Stephens (1991), A new polarized atmospheric radiative transfer model, *J. Quant. Spectrosc. Radiat. Transfer*, *46*, 413–423.

Gérard, B., J. L. Deuzé, M. Herman, Y. J. Kaufman, P. Lallart, C. Oudard, L. A. Remer, B. Rogers, B. Six, and D. Tanré (2005), Comparison

between POLDER 2 and MODIS/Terra aerosol retrievals, *J. Geophys. Res.*, *110*, D24211, doi:10.1029/2005JD006218.

Hagolle, O., P. Goloub, P. Y. Deschamps, H. Cosnefroy, X. Briottet, T. Bailleul, J. M. Nicolas, F. Parol, B. Lafrance, and M. Herman (1999), Results of POLDER in-flight calibration, *IEEE Trans. Geosci. Remote Sens.*, *37*, 1550–1566.

Hansen, J., and L. Travis (1974), Light scattering in planetary atmospheres, *Space Sci. Rev.*, *16*, 527–610.

Hasekamp, O. P., and J. Landgraf (2005), Retrieval of aerosol properties over the ocean, *J. Geophys. Res.*, *110*, D20207, doi:10.1029/2005JD006212.

Hasekamp, O. P., and J. Landgraf (2007), Retrieval of aerosol properties over land surfaces: Capabilities of multiple-viewing-angle intensity and polarization measurements, *Appl. Opt.*, *46*, 3332–3344.

Ignatov, A., and L. Stowe (2000), Aerosol retrievals from individual AVHRR channels. Part I: Retrieval algorithm and transition from dave to 6S radiative transfer model, *J. Atmos. Sci.*, *59*, 313–334.

Intergovernmental Panel on Climate Change (2001), *Climate Change 2001: The Scientific Basis—Contribution of Working Group I to the Third Assessment Report of the Intergovernmental Panel on Climate Change*, edited by J. R. Houghton et al., Cambridge Univ. Press, New York.

Kahn, R., R. West, D. McDonald, B. Rheingans, and M. I. Mishchenko (1997), Sensitivity of multiangle remote sensing observations to aerosol sphericity, *J. Geophys. Res.*, *102*, 16,861–16,870.

Kahn, R. A., B. J. Gaitley, J. V. Martonchik, D. J. Diner, and K. A. Crean (2005), Multiangle Imaging SpectroRadiometer (MISR) global aerosol optical depth validation based on two years of coincident Aerosol Robotic Network (AERONET) observations, *J. Geophys. Res.*, *110*, D10S04, doi:10.1029/2004JD004706.

King, M. D., Y. J. Kaufman, D. Tanré, and T. Nakajima (1999), Remote sensing of tropospheric aerosols from space: past, present and future, *Bull. Am. Meteorol. Soc.*, *80*, 2229–2259.

Koepke, P. (1984), Effective reflectance of oceanic white caps, *Appl. Opt.*, *23*, 1816–1824.

Mishchenko, M. I., and L. D. Travis (1997), Satellite retrieval of aerosol properties over the ocean using polarization as well as intensity of reflected sunlight, *J. Geophys. Res.*, *102*, 13,543–13,553.

Mishchenko, M. I., L. D. Travis, W. B. Rossow, B. Cairns, B. E. Carlson, and Q. Han (1997), Retrieving CCN column density from single-channel measurements of reflected sunlight over the ocean: A sensitivity study, *Geophys. Res. Lett.*, *24*, 2655–2658.

Mishchenko, M. I., B. Cairns, J. E. Hansen, L. D. Travis, R. Burg, Y. J. Kaufman, J. V. Martins, and E. P. Shettle (2004), Monitoring of aerosol forcing of climate from space: Analysis of measurement requirements, *J. Quant. Spectrosc. Radiat. Transfer*, *88*, 149–161, doi:10.1016/j.jqsrt.2004.03.030.

Mishchenko, M. I., B. Cairns, J. Chowdhary, I. V. Geogdzhayev, L. Liu, and L. D. Travis (2005), Remote sensing of terrestrial tropospheric aerosols from aircraft and satellites, *J. Physics*, *6*, 73–89, doi:10.1088/1742-6596/6/1/005.

Mishchenko, M. I., B. Cairns, G. Kopp, C. F. Schueler, B. A. Fafaul, J. E. Hansen, R. J. Hooker, T. Itchkawich, H. B. Maring, and L. D. Travis (2007), Precise and accurate monitoring of terrestrial aerosols and total solar irradiance: Introducing the Glory Mission, *Bull. Am. Meteorol. Soc.*, *88*, 677–691.

Monahan, A. H. (2006), The probability distribution of sea surface wind speeds. Part I: Theory and SeaWinds observations, *J. Clim.*, *19*, 497–520.

Moody, E. G., M. D. King, S. Platnick, C. B. Schaaf, and F. Gao (2004), Spatially complete global spectral surface albedos: Value-added datasets derived from Terra MODIS land products, *IEEE Trans. Geosci. Remote Sens.*, *43*, 144–158, doi:10.1109/TGRS.2004.838359.

Moody, E. G., M. D. King, S. Platnick, C. B. Schaaf, and F. Gao (2005), Spatially complete global spectral surface albedos: Value-added datasets derived from Terra MODIS land products, *IEEE Trans. Geosci. Remote Sens.*, *43*, 144–158.

Morel, A. (1988), Optical modeling of the upper ocean in relation to its biogenous water content (case I waters), *J. Geophys. Res.*, *93*, 10,749–10,768.

Nadal, F., and F. Bréon (1999), Parameterization of surface polarized reflectance derived from POLDER spaceborne measurements, *IEEE Trans. Geosci. Remote Sens.*, *37*, 1709–1718.

Rodgers, C. (2000), *Inverse Methods For Atmospheric Sounding: Theory and Practice*, World Sci., Hackensack, N. J.

Schwartz, S. (2004), *Aerosols, Clouds and Climate Change, Nucleation and Atmospheric Aerosols*, edited by M. Kashahara and M. Kulmala, pp. 323–338, Kyoto Univ. Press, Kyoto, Japan.

Smirnov, A., B. N. Holben, Y. J. Kaufman, O. Dubovik, T. F. Eck, I. Slutsker, C. Pietras, and R. Halthore (2002), Optical properties of atmospheric aerosol in maritime environments, *J. Atmos. Sci.*, *59*, 501–523.

Stephens, G. L., et al. (2002), The CloudSat mission and the A-Train, *Bull. Am. Meteorol. Soc.*, *83*, 1771–1790.

Tanré, D., M. Herman, and Y. J. Kaufman (1996), Information on aerosol size distribution contained in solar reflected spectral radiances, *J. Geophys. Res.*, *101*(D14), 19,043–19,060.

Tanré, D., Y. J. Kaufman, M. Herman, and S. Mattoo (1997), Remote sensing of aerosol properties over oceans using the MODIS/EOS spectral radiances, *J. Geophys. Res.*, *102*, 16,971–16,988.

Twomey, S. (1977), The influence of pollution on the shortwave albedo of clouds, *J. Atmos. Sci.*, *34*, 1149–1152.

Van De Hulst, H. C. (1981), *Light Scattering by Small Particles*, Dover, Mineola, N. Y.

M. Lebsock, T. S. L'Ecuyer, and G. L. Stephens, Department of Atmospheric Science, Colorado State University, Fort Collins, CO 80523-1371, USA. (lebsock@atmos.colostate.edu)